

Attosecond Control of Squeezed Light

Russell Zimmerman^{†, 1} Shashank Kumar^{†, 1, a)} Shiva Kant Tiwari,² Eric Liu,¹ Francis Walz,¹ Siddhant Pandey,¹ George J. Economou II,¹ Hadiseh Alaeian,^{3, 1, 4} Chen-Ting Liao,⁵ Valentin Walther,^{1, 4, 2} and Niranjan Shivarayam^{1, 4, b)}

¹⁾Department of Physics and Astronomy, Purdue University, 525 Northwestern Ave., West Lafayette, 47907, Indiana, USA

²⁾Department of Chemistry, Purdue University, 560 Oval Dr, West Lafayette, IN 47907, West Lafayette, 47907, Indiana, USA

³⁾Elmore Family School of Electrical and Computer Engineering, 465 Northwestern Ave., West Lafayette, Indiana 47907, USA

⁴⁾Purdue Quantum Science and Engineering Institute, 1205 W State St, West Lafayette, Indiana 47907, USA

⁵⁾Department of Physics, Indiana University Bloomington, 727 E. Third St., Bloomington, 47405, Indiana, USA

Squeezed light has revolutionized quantum metrology by enhancing interferometry for sensitive applications such as the detection of gravitational waves. Squeezed light has also played a pivotal role in quantum information science with numerous applications in quantum computing and communication. Previously, squeezed light has been primarily generated using nonlinear optical interactions, where control of the degree of squeezing was possible by tuning the nonlinearity of the generating medium using suitable material engineering. Here, we modulate the third-order nonlinear response in dielectrics with strong ultrafast laser fields to control the degree of squeezing on attosecond time scales. We demonstrate the ability to change the ultrafast squeezed light generated in the nonlinear process from amplitude-squeezed to phase-squeezed by controlling the strong-field-driven nonlinear response of the material through a sub-cycle phase delay between the input femtosecond laser pulses. The squeezing of quantum noise is measured using a frequency-resolved balanced homodyne detection scheme capable of extracting the field quadratures in different frequency modes simultaneously. Using this frequency-resolved measurement we extract the complete coherency matrix containing the quantum correlations between field quadratures across different frequency modes of the femtosecond squeezed light pulse. These results have major implications for the development of quantum light sources with unprecedented levels of control over quadrature squeezing, for applications in multi-mode quantum information processing, and for measuring transient quantum matter correlations via transduction to quantum field correlations in an ultrafast light-matter interaction.

Keywords: Attosecond, Squeezed Light, Quantum Correlations, Nonlinear Response

[†]These authors contributed equally to this work.

INTRODUCTION

Squeezed light is a crucial component in a variety of quantum applications ranging from quantum metrology to quantum information science¹. At the Laser Interferometer Gravitational Wave Observatory (LIGO), squeezed light has been utilized to reduce shot noise below the quantum limit, which allows for unprecedented sensitivity of gravitational waves^{2–5}. In the field of quantum computing, the relevance of squeezed light to continuous-variable quantum information processing allows a better understanding of dense coding and universal quantum computing^{6,7}. Exploiting the quantum states of light is also useful in imaging applications to reach resolution beyond the classical limit^{8,9}. Squeezed light with its quadrature noise below the quantum noise limit is fundamental in enhancing both laser interferometry¹⁰ as well as spectroscopy¹¹. Despite achieving initial generation nearly four decades ago, squeezed light has primarily been generated with continuous-wave lasers^{12–14}. In addition to squeezed light, other quantum states of light have been generated, such as optical Schrödinger’s cat states, which are superpositions of two coherent states^{15,16}. These

^{a)}Electronic mail: kumar414@purdue.edu

^{b)}Electronic mail: niranjan@purdue.edu

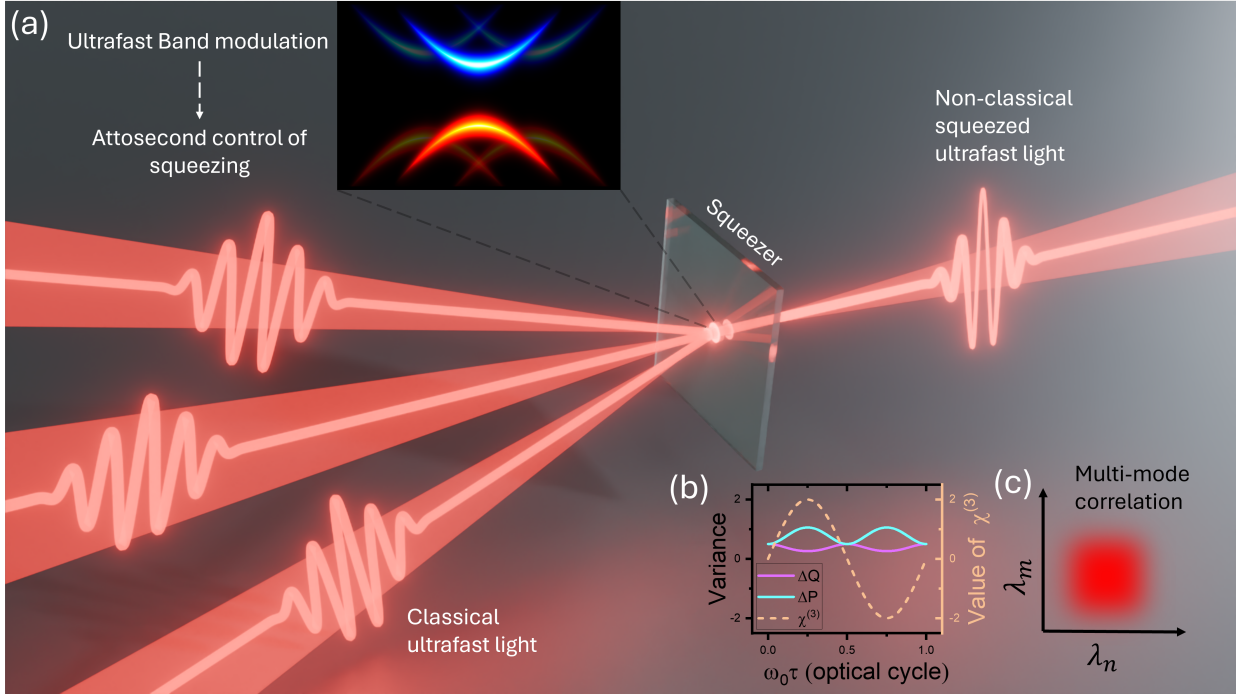


FIG. 1. Concept and Experimental Scheme: (a) Three femtosecond pulses interact with a large band-gap dielectric (MgO) and generate a four-wave mixing signal exhibiting quadrature squeezing. The four-wave mixing process occurs simultaneously with a modulation of the material band-structure (inset in (a)) driven by the strong electric field of the laser pulses. This band modulation results in attosecond scale control of the degree and type of quadrature squeezing. The quantum state of this broadband squeezed light is measured with a frequency-resolved homodyne tomography technique revealing multi-frequency mode quadrature correlations in the generated ultrafast squeezed light. (b) shows quadrature variance modulation from theory and (c) a schematic of quadrature correlations between different frequency modes that can be extracted from the experiment.

experiments use homodyne detection and have primarily remained within the continuous-wave laser regime, though recent experiments have measured these cat states from ultrafast lasers¹⁶.

While continuous-wave squeezed light sources have been available for a few decades, the generation and measurement of ultrafast squeezed light on the femtosecond and attosecond scale is still in its infancy. Bright squeezed vacuum states have been generated with ultrashort pulses^{17,18} and, more recently, have been used to drive high harmonic generation in solids¹⁹ and gases²⁰. Compared to continuous-wave lasers, ultrafast lasers present additional challenges, such as difficulty in spatial mode cleaning and decreased power stability of the laser. Alongside these challenges, ultrafast lasers also offer new opportunities for quantum light generation with their inherent frequency multi-mode properties due to their broad bandwidth in addition to their strong fields capable of manipulating the nonlinear response of materials used to generate such quantum light. In the femtosecond regime, squeezed vacuum has been generated and measured in the time-domain on a sub-cycle scale using electro-optic sampling²¹. Recently, few-cycle femtosecond pulses at visible and near infrared wavelengths were used to generate ultrafast squeezed light measured by spectral interferometry, where the Wigner distributions of the squeezed light and the degree of squeezing were inferred by comparison with theory²². Furthermore, complete quantum state tomography of extreme-ultraviolet light from high harmonic generation has now been demonstrated²³.

Nonlinear optical interactions typically result in the generation of quantum light^{24–26}. Using such interactions quantum light demonstrating quadrature squeezing has been generated via degenerate four-wave mixing (DFWM)^{27–30} and second harmonic generation³¹. Despite major advances in squeezed light generation, ultrafast nonlinear interactions that determine its transient non-classical properties including the potential for attosecond dynamical control have not been explored. Achieving a high degree of control over the properties of squeezed light and the capabilities to measure quantum correlations on attosecond time scales could greatly benefit the emerging field of attosecond quantum optics. Here, we describe an experiment

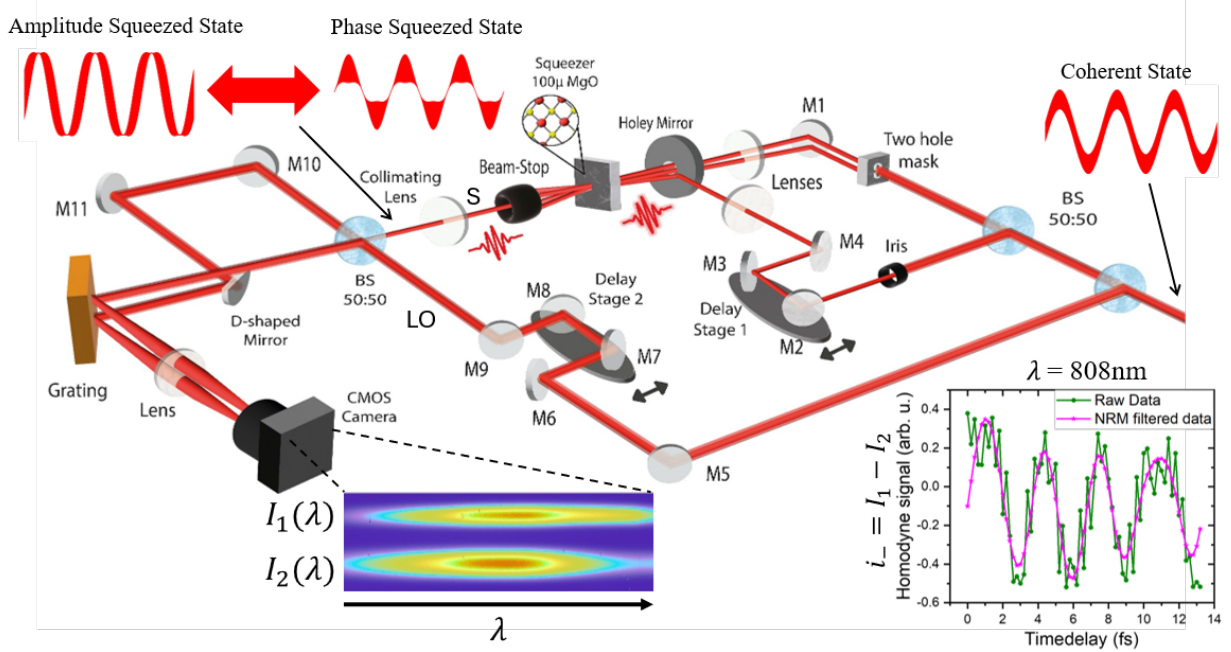


FIG. 2. Schematic of ultrafast squeezed light generation with attosecond control and frequency-resolved balanced homodyne detection using a grating spectrometer. A 50-fs laser beam is split to form the local oscillator and a squeezed light generation beam. The squeezed light is generated using a degenerate four-wave mixing (DFWM) scheme using three beams created using a second beamsplitter and a two-hole mask. The DFWM interaction occurs in a 100 micron thick MgO target (squeezer) placed at the focus. The DFWM signal beam (squeezed light) is collimated using a lens and sent to the balanced homodyne setup, where it is combined with the local oscillator using a beamsplitter. The transmitted and reflected beams from the beamsplitter propagate to a diffraction grating, and the resulting spectra are imaged with a CMOS camera. Delay stage 1 introduces an attosecond-scale time delay (τ) between the DFWM pulses for attosecond squeezing control. The phase delay (ϕ_{LO}) between the squeezed light and the local oscillator is scanned using delay stage 2. BS: 50/50 beamsplitter.

to generate, measure, and control ultrafast squeezed light from DFWM in magnesium oxide (see figure 1). We demonstrate sub-cycle, attosecond-scale control of both the degree of squeezing and the type of quadrature squeezing. The switching of squeezing between the amplitude and phase quadratures is prominently observed. This control over squeezed light generation is achieved using a strong-field-driven nonlinear response modulation (NRM) in the generating material³². We completely characterize the generated ultrafast squeezed light pulse using frequency-resolved balanced homodyne detection (FR-BHD). This FR-BHD is achieved using a modulation of the nonlinear response of the squeezing medium induced by varying the time delay between the input DFWM pulses. Such a strong-field-driven modulation of the nonlinear response modulates the generated broadband squeezed light and is used as a filter to suppress electronic noise and measure frequency-resolved squeezing below the shot-noise limit of the laser light. In contrast to balanced photodiode measurements, the filtering process demonstrated here (henceforth called NRM filtering) enables homodyne tomography measurements at the quantum noise limit with a CMOS camera, which has not been previously possible. Furthermore, our FR-BHD measurement provides access to quadrature correlations between different frequency modes measured simultaneously. This in turn allows direct extraction of the coherency matrix and helps us determine the principal modes contributing to our squeezed light pulse³³. In previous work, frequency multiplexing has been utilized to measure correlations between different frequency modes in squeezed light generated in an optical parametric oscillator³⁴. Our approach goes beyond such multiplexing techniques by offering a path to measure dynamical quadrature correlations to study ultrafast quantum dynamics.

EXPERIMENT

Figure 2 illustrates the experimental setup for the generation of ultrafast squeezed light with attosecond control and frequency-resolved balanced homodyne detection. Squeezed light is generated by a Degenerate Four-Wave Mixing (DFWM) interaction of three non-collinear near-infrared (NIR) femtosecond laser pulses with a $100 \mu\text{m}$ thick magnesium oxide sample. The generated signal is sent to a balanced homodyne detection setup that incorporates a diffraction grating and a standard CMOS camera for frequency-resolved detection (see Methods). To perform frequency-resolved balanced homodyne detection, the spectra from the two arms of the homodyne detection setup are subtracted for each wavelength. Although the pixels on the camera corresponding to the same wavelength in each spectrum are similar, they do not have well-matched noise characteristics. As a result, balanced detection sufficient to reach the quantum noise limit of the laser cannot be reached. We overcome this limitation by utilizing a strong-field-driven modulation of the material's nonlinear response³² and filtering the squeezed light signal based on this modulation, as described below.

Nonlinear Response Modulation

In perturbative nonlinear optics, the nonlinear response functions of a material (nonlinear susceptibilities) depend only on material properties and are independent of external fields. However, when moderately strong laser fields similar to field strengths used in solid-state high-order harmonic generation (HHG)³⁵, which are typically in the $10^{11} - 10^{12} \text{ W/cm}^2$ range, are applied, the nonlinear susceptibilities are modified by the external fields. When generating squeezed light from DFWM, the properties of squeezed light such as the degree of squeezing are directly related to third-order susceptibility^{36,37}. Hence, a strong-field-driven modulation of this susceptibility leads to attosecond control over the generated squeezed light. We note that periodic modulation of pump light in a nonlinear optical cavity has been proposed to generate highly squeezed light³⁸ but field driven nonlinear response modulation has not been previously explored. In our work, we show that in addition to attosecond control, quantum noise level can be reached in frequency-resolved balanced homodyne detection measurements using a CMOS camera by leveraging this nonlinear response modulation.

When the time delay between the phase-locked gate pulses and the probe pulse is varied on sub-cycle time scales, the total electric field at a given point in the focal volume modulates because of constructive and destructive interference. This modulation of the total field modulates the nonlinear response of the material³², resulting in modulation of the generated squeezed light. Figure 2 inset (bottom right corner) shows the homodyne signal as a function of time delay (τ) for a fixed relative phase (ϕ_{LO}) of the local oscillator with respect to the signal. We use a low-pass filter that filters out any time-delay frequencies higher than $1\omega_0$, where ω_0 is the frequency corresponding to the central wavelength of 808 nm. The details of this filtering process are explained in the supplementary material.

Quantum Tomography and Attosecond Control of Quadrature Squeezing

The NRM-filtered homodyne detection technique is employed to directly measure the ϕ_{LO} phase-dependent generalized quadratures of the DFWM output signal. Using optical homodyne tomography, we reconstruct the Wigner distribution function of the DFWM signal^{13,39}. We use the inverse Radon transformation to obtain the Wigner functions from the measurement of homodyne signal. Details of the reconstruction algorithm are provided in the Methods section. The Wigner distributions were constructed for all time delays (τ) using both raw (unfiltered) and NRM-filtered data. Figures 3 (a) and (b) show the Wigner functions corresponding to time delays of $\tau = 5.4 \text{ fs}$ and 10.2 fs respectively for 808 nm, obtained from the data without NRM filtering, while Figs. 3 (c) and (d) show the corresponding NRM-filtered results. The Wigner functions are shown for the central wavelength (808 nm) of the output signal. Amplitude-squeezing and phase-squeezing are prominently observed along with the negativity of the Wigner function, indicating the non-classical nature of the generated light⁴⁰. The shift in the centroid of the Wigner distribution with time delay arises from the change in the global phase of the DFWM signal with respect to the local oscillator, which cannot be compensated for in the current experimental configuration. To quantify the degree of squeezing, we fit a two-dimensional Gaussian function to the Wigner functions and extract the maximum

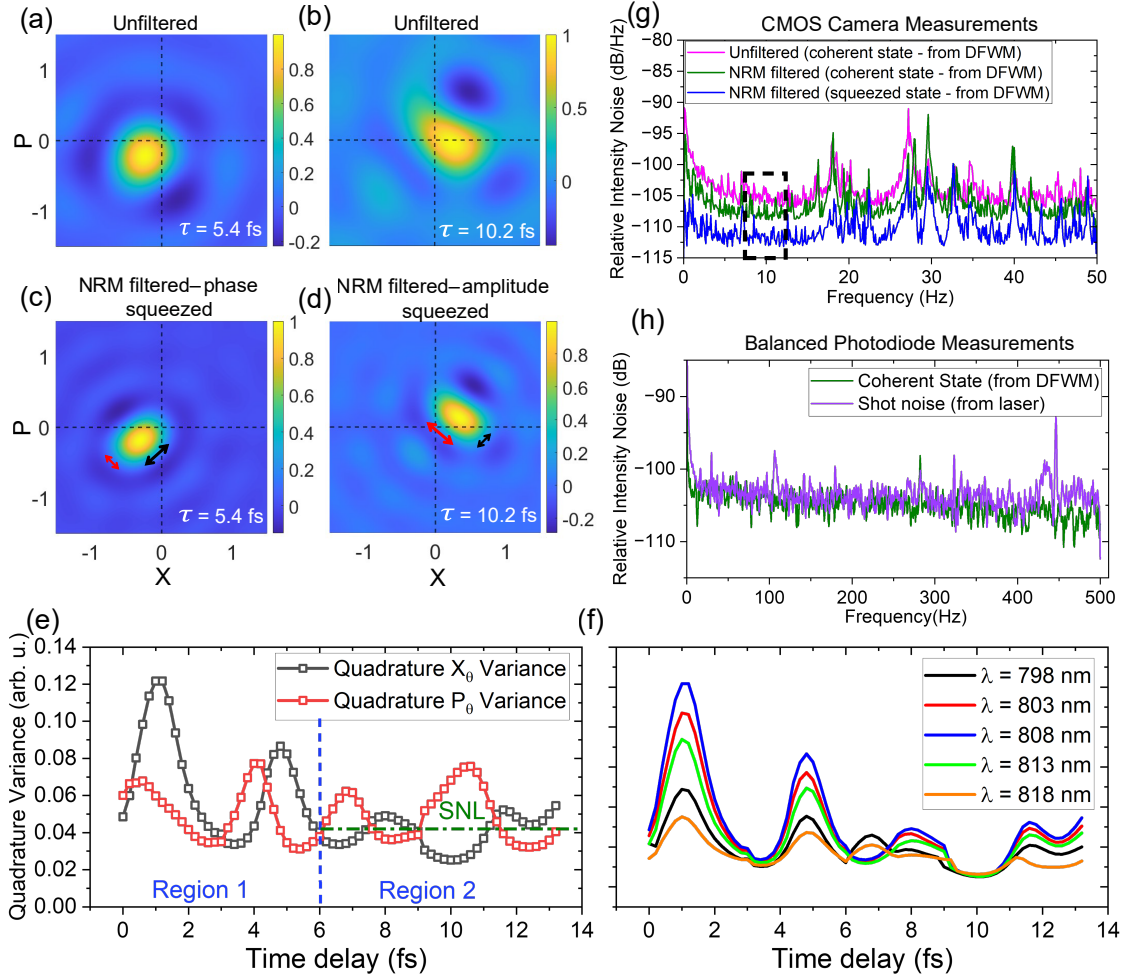


FIG. 3. The normalized Wigner distribution function obtained from the homodyne signal for time delays (a) $\tau = 5.4$ fs and (b) $\tau = 10.2$ fs. The NRM-filtered Wigner functions are shown in (c) for $\tau = 5.4$ fs and in (d) for $\tau = 10.2$ fs. Negativity of the Wigner function is seen in (c) and (d) indicating non-classical nature of the measured light. The NRM-filtered Wigner function for 808 nm is then fitted to a 2D Gaussian function. The variances of the 2D Gaussian function are extracted using the fitting procedure for each time delay and shown in (e). The quadrature variances shown in (e) corresponding to time delays shown in (c) and (d) are indicated with red and black arrows in the Wigner plots. X_θ and P_θ are generalized quadratures. The rapidly varying and constant shot noise level (SNL) regions are separated using a blue dashed line as Region 1 and Region 2, respectively (see the main text for details). (f) shows the oscillation of the maximum and minimum variances as a function of time delay for different wavelengths within the bandwidth of the squeezed light pulse. These oscillations at different wavelengths are observed to be synchronized in-phase. The relative intensity noise (RIN) for unfiltered coherent state (magenta), NRM-filtered coherent state (green), and NRM-filtered squeezed state (blue) are obtained using the power spectral density of the homodyne signal at time delay $\tau = 7.6$ fs (coherent) and $\tau = 10.2$ fs (squeezed). These RIN measurements performed using the CMOS camera are shown in (g). The quadrature noise of the coherent state obtained using the homodyne signal measurement is compared with the shot noise level of the laser using standard balanced photodiode detectors, and shown in (h). The overlap of the coherent state RIN with the laser shot noise RIN in (h) shows that the coherent state RIN in (g) corresponds to the shot-noise level and that squeezing is measured below the shot-noise limit.

and minimum variances at each time delay for generalized quadratures X_θ and P_θ . Figure 3 (e) shows the modulation of the degree of squeezing as a function of time delay extracted using the fitting procedure. Figure 3 (e) is divided into two regions, Region 1 and Region 2. We do not observe a constant shot noise level (point of intersection of the red and black curves) in Region 1 likely due to experimental instability as well as rapid variation in signal intensity near zero delay as compared to Region 2. In Region 2 the shot noise

is measured to be constant and well defined. Using homodyne detection of the nonlinear DFWM process driven by ultrafast femtosecond pulses, we have demonstrated that the squeezing of the output signal can be controlled with unprecedented temporal resolution on the sub-cycle attosecond scale via the controlled modulation of third-order nonlinear susceptibility, $\chi^{(3)}$, of the material. Such fine control over the properties of squeezed light could have major applications in attosecond quantum optics where quantum light is being used to drive processes such as HHG^{20,23} and multiphoton ionization⁴¹.

To provide further evidence that we are observing squeezing below the quantum noise limit, we performed a quantum noise analysis of the measured homodyne signal using the measured power spectral density (PSD). The relative intensity noise (RIN) was calculated from the raw, unfiltered data for a near-coherent state at $\tau = 7.4$ fs, where the variances in both quadratures are nearly equal, and is plotted in Fig. 3 (g) (magenta). The corresponding RIN for the NRM-filtered data of the near-coherent state is shown in green in Fig. 3 (g). We show that by applying the NRM filter, the quantum noise in our measurements can be reduced by a few decibels (dB). The RIN of the signal corresponding to maximum squeezing (at $\tau = 10.2$ fs) is plotted in blue in Fig. 3 (g). This shows that the quantum noise of the squeezed state lies several dB below that of the coherent state. Since direct shot-noise measurements are not possible using a CMOS camera, we repeat the experiment using a balanced photodiode detector to measure the homodyne signal. The quadrature noise was measured over the full spectral range of the DFWM signal. The measured quadrature noise for the coherent state at $\tau = 7.4$ fs overlaps with the laser's shot-noise limit, as shown in Fig. 3 (h), confirming that the noise in the near-coherent state approaches the fundamental shot-noise limit of the laser pulse. Since Fig. 3 (g) clearly shows that the squeezed-state noise lies below that of the near-coherent state, the degree of quantum noise reduction in the squeezed state can thus be quantitatively established. To estimate the maximum degree of squeezing achieved in this experiment, we integrate the RIN of the NRM-filtered coherent and squeezed states around the 10 Hz frequency region (see the dashed rectangular box in Fig. 3 (g)). In this low electronic-noise frequency region, the RIN of the squeezed light reaches a value corresponding to a degree of squeezing of ~ 5 dB.

Multi-mode Quadrature Correlations

As discussed earlier, one of the key advantages of using a spectrometer for detection is that it enables frequency-resolved measurement of the homodyne signal. This allows us to access the quantum state of the emitted signal across different frequency modes. Moreover, because all frequency components are recorded simultaneously within a single shot, it is possible to extract quadrature correlations between these frequency modes. We thus analyze the homodyne signal across different frequency components and perform optical homodyne tomography to reconstruct the corresponding Wigner functions. The Gaussian fitting procedure is then applied to extract the quadrature variances for each frequency mode. Figure 3 (f) shows the modulation of the quadrature variance as a function of time delay for several selected wavelengths near the central wavelength $\lambda = 808$ nm. As we deviate from the central wavelength, the degree of squeezing reduces, however, the variance oscillations are completely in-phase, demonstrating strong correlations between different frequency modes.

For a multimode quantum state, the information on quantum correlations is contained within the quantum coherency and quantum covariance matrices. The coherency matrix is defined as³³

$$(\Gamma^{(1)})_{mn} = \langle \hat{a}_m^\dagger \hat{a}_n \rangle \quad (1)$$

where $\hat{a}_m^\dagger(\hat{a}_m)$ is the creation (annihilation) operator of a photon in frequency mode m . The second-order moments of the field quadratures are contained in the covariance matrix, defined³³

$$\Sigma = \begin{pmatrix} \langle \hat{X}_m \hat{X}_n \rangle & \langle \hat{X}_m \hat{P}_n \rangle \\ \langle \hat{P}_m \hat{X}_n \rangle & \langle \hat{P}_m \hat{P}_n \rangle \end{pmatrix} \quad (2)$$

In our homodyne experiment, we directly measure the quadratures X_m and P_m of different frequency modes simultaneously. Consequently, the complete covariance matrix can be reconstructed from the experimentally acquired data. The coherency matrix can further be calculated from the quadrature correlations using the relation³³

$$(\Gamma^{(1)})_{mn} = \frac{1}{4} \left[\langle \hat{X}_m \hat{X}_n \rangle + \langle \hat{P}_m \hat{P}_n \rangle + i(\langle \hat{X}_m \hat{P}_n \rangle - \langle \hat{P}_m \hat{X}_n \rangle) \right] \quad (3)$$

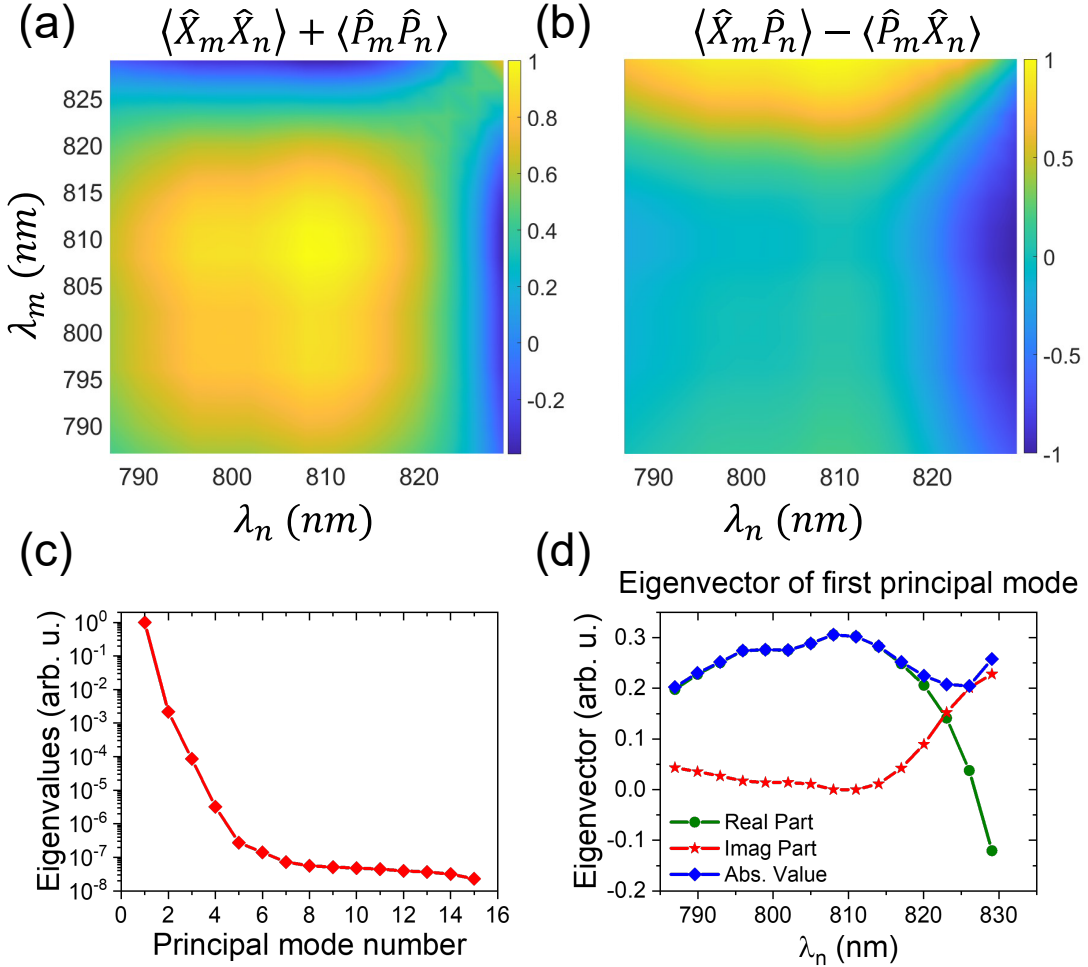


FIG. 4. The correlation functions (a) $\langle \hat{X}_m \hat{X}_n \rangle + \langle \hat{P}_m \hat{P}_n \rangle$ and (b) $\langle \hat{X}_m \hat{P}_n \rangle - \langle \hat{P}_m \hat{X}_n \rangle$ are shown, where m and n denote the frequency modes. Here, X represents the quadrature along the direction of maximum squeezing, and P is the conjugate quadrature orthogonal to X , evaluated for the Wigner function at $\tau = 10.2$ fs. From these correlation functions, the coherency matrix is constructed (see Eq. 3). The eigenvalues of the coherency matrix, obtained via diagonalization, are shown in (c). The eigenvector corresponding to the dominant first principal mode, presented in (d), reveals that this mode constitutes a linear combination of multiple frequency components with approximately equal weights.

Fig. 4 (a) and (b) show the real and imaginary part of the coherency matrix. Diagonalization of the coherency matrix yields the principal eigenmodes. The eigenvalues of the coherency matrix are shown in Fig. 4 (c) and represent the mean photon numbers in each principal mode. Before the interaction with the material, the coherent state is confined to a single principal mode. Following the DFWM interaction, mode mixing occurs, leading to the generation of a multimode squeezed state of light. The large eigenvalue of the first principal mode seen in Figure 4 (c) indicates that although intermodal coupling is present, the output quantum field remains predominantly governed by the first principal mode. The eigenvector corresponding to the first principal mode shown in Fig. 4 (d) indicates that the first principal mode is a linear combination of all frequencies with approximately equal weights.

It has been well established that the quantum properties of light are influenced by the nonlinear response of the material through which it propagates. In particular, for nonlinear optical processes such as degenerate four-wave mixing, non-classical features including the squeezing parameter are directly determined by the material's third-order susceptibility^{25,36,37}. However, when strong femtosecond laser fields participate in the wave-mixing process, the electronic configuration of the medium is non-perturbatively modified in the

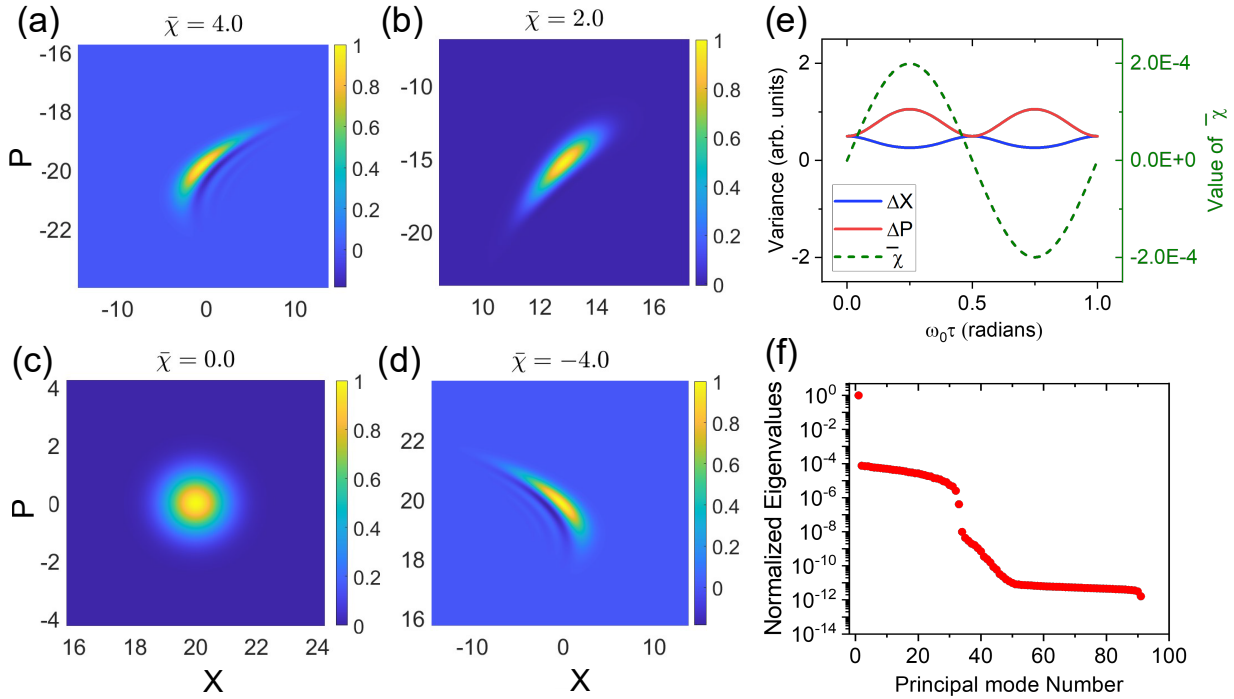


FIG. 5. The Wigner distributions calculated using the nonlinear Schrödinger equation (see Eq. 15) are shown for different values of the dimensionless coupling constant $\bar{\chi}$ (a) 4, (b) 2, (c) 0, and (d) -4. Panel (e) illustrates that modulation of $\bar{\chi}$ leads to corresponding modulation in the variances of the generalized quadratures. The eigenvalues of the calculated coherency matrix are shown in panel (f), indicating that the photon population is predominantly confined to the first principal mode, with only minor contributions from higher-order modes. This result is consistent with the principal mode decomposition obtained from the experimentally measured data.

presence of the field. In solid-state systems, this effect arises from strong-field-induced modulation of the electronic band structure⁴²⁻⁴⁴. In a recent study, it has been shown that the third-order susceptibility is modulated by changing the time delay between the input femtosecond pulses³².

Though a complete simulation of the quantum optical interaction in the presence of strong fields is currently very challenging, we phenomenologically introduce the modulation of susceptibility into an existing quantum optical model to describe the quantum state of the output signal. We simulate the quantum state of light of the output signal in the four-wave mixing process by solving the effective one-dimensional nonlinear Schrödinger's equation for the photon field propagating through a nonlinear medium (see Methods). We then parameterize the dimensionless coupling constant $\bar{\chi}$ (proportional to third-order susceptibility) with time delay between the input pulses. The full numerical solution of the quantum light field after propagation through the crystal is well approximated by the nonlinear evolution of its first principal mode, which can be solved analytically (see Methods). The computed Wigner distribution functions display negative components of the Wigner function characteristic of non-classical light (Fig. 5 (a) - (d)). The dependence on $\bar{\chi}$ clearly illustrates that the degree and type of squeezing varies with the coupling strength. Furthermore, we show in Fig. 5 (e) that a periodic modulation of $\bar{\chi}$ modulates the variance of the generalized quadratures X_θ and P_θ . In our calculations, $\bar{\chi}$ is independent of frequency because the third-order susceptibility in the experiment is expected to be constant over the bandwidth of our laser pulse for a large band-gap dielectric such as MgO. This assumption is also consistent with our experimentally extracted frequency-frequency correlations that are nearly constant over the full bandwidth (see Fig. 4). Our effective model thus captures the main emergent quantum light features, including the single-mode character and quadrature variance oscillations, allowing a simple, semi-analytic analysis of the results. A complete quantitative model would require a quantum optical description of strong field driven processes in a dielectric.

In conclusion, we have experimentally demonstrated sub-cycle, attosecond control of ultrafast femtosecond squeezed light generation from a nonlinear optical process. We have measured quadrature correlations

between different frequency modes simultaneously across the full bandwidth of the femtosecond pulse. This was made possible by a fundamentally new approach towards generation and measurement of field quadrature squeezing by leveraging strong-field driven modulation of the nonlinear response in a large band-gap dielectric³², which allows us to reach the quantum noise limit using an unbalanced CMOS detector. From our experimental measurements, we directly construct Wigner distribution functions representing the full quantum state of the DFWM signal, which prominently shows control over the degree and type of squeezing as the time delay is varied with attosecond resolution. Furthermore, using the simultaneous measurement of field quadratures in multiple frequency modes, we have constructed the coherency matrix and determined that a single principal mode is dominant in the generated squeezed light. Our work is a major step towards generating, measuring, and using ultrafast squeezed light at high power levels necessary for applications such as high-harmonic generation and multiphoton ionization in attosecond quantum optics, where non-classical light with sub-cycle temporal control could open new opportunities^{19,41,45,46}. The demonstrated control of squeezing due to strong-field enhanced nonlinear response could push the limits of achievable squeezing with numerous applications in quantum metrology^{10,11} and quantum information science^{6,34}. Finally, multi-mode correlation measurements at the quantum noise limit could open a new paradigm for transduction of dynamical quantum correlations in matter to quantum correlations in electric fields on attosecond time scales.

METHODS

Experimental Setup

The generation and measurement scheme of our squeezed light signal is shown in Fig. 2 and employs degenerate four-wave mixing (DFWM) coupled with a strong local oscillator to achieve homodyne detection. 50 fs pulses with a center wavelength 808 nm from a 1 kHz repetition rate Ti:Sapph laser are first split using a 50/50 beam splitter. The reflected arm becomes the local oscillator and is sent to delay stage 2 to control relative phase, ϕ_{LO} , between the signal (squeezed light) and the local oscillator in 100 steps per optical cycle with a step size of 27 attoseconds. The transmitted arm is further separated into two phase-locked gate beams and a probe beam using a beam splitter and a two-hole mask. Time delay, τ , between the two gate beams and the probe beam is controlled via delay stage 1 with a delay resolution of approximately 200 attoseconds. The probe and gate beams, with average intensities of $\sim 2 \text{ TW/cm}^2$ and $\sim 1 \text{ TW/cm}^2$, respectively, interact with a 100 μm thick sample of MgO (100) via a BOXCARS⁴⁷ configuration to generate the squeezed signal. All input beams are spatially filtered using an iris. The resulting signal beam is spatially isolated from the input beams and coupled to the local oscillator via a typical homodyne measurement beam path with a power ratio of approximately 40:1. As seen in Fig. 2, we use a diffraction grating with 1500 grooves/mm and a CMOS camera to make a spectrally-resolved homodyne measurement. For this two-dimensional scan (τ and ϕ_{LO}) 1000 single shots of both paths are simultaneously captured at a frame rate of 100 Hz at each delay position. Our spectrometer has a calibrated spectral resolution of 0.06 nm per pixel. Isolation of individual frequency modes, as well as implementation of nonlinear response modulation filtering, allows this measurement with a CMOS detector to reach the shot noise limit without the necessity of balanced integrated circuitry normally seen in a balanced photodiode system of homodyne detection²⁴.

Optical Homodyne Tomography

We sampled 1000 laser shots of the homodyne signal for each ϕ_{LO} and τ and constructed the probability distribution function (PDF) of the homodyne signal (i_-). To reconstruct the Wigner function, an inverse Radon transformation is performed^{13,39},

$$W_\tau(Q, P) = \frac{1}{4\pi^2} \iint \int_0^\pi pr_\tau(s, \phi) \exp[-i\eta(s - Q \cos \phi - P \sin \phi)] d\eta ds d\phi \quad (4)$$

where $pr_\tau(s, \phi)$ is the PDF of the homodyne signal in various phases of $\phi = \phi_{LO}$, and τ is the time delay between gate and probe pulses, which parameterizes the PDF. s is the laser shot index and η is the variable which defines the kernel of the Radon transformation. Figures 3 (a)-(d) show the Wigner distribution

functions of the DFWM signal in generalized quadrature X and P for two different values of time delay τ using raw and NRM-filtered data (see supplementary material for the NRM filtering procedure). To estimate the amplitude and phase variances of the constructed Wigner function, we fit a generalized 2D Gaussian function⁴⁸,

$$W(r_1, r_2) = \exp\left(-\frac{(r_1 - d_1)^2}{2V_1}\right) \exp\left(-\frac{(r_2 - d_2)^2}{2V_2}\right) \quad (5)$$

where, $\begin{pmatrix} r_1 \\ r_2 \end{pmatrix} = \begin{pmatrix} \cos \theta & -\sin \theta \\ \sin \theta & \cos \theta \end{pmatrix} \begin{pmatrix} Q \\ P \end{pmatrix}$ is the rotated coordinate system and (d_1, d_2) is the displacement vector in the rotated system. The parameters V_1 and V_2 represent the variance of the distribution along the respective direction r_1 and r_2 . Using the fitting procedure, the values of V_1 and V_2 are extracted for every time delay and plotted in Fig. 3 (g). It is seen that the variances along r_1 and r_2 generalized direction modulate with the time delay between gate and probe pulses with attosecond resolution.

Theory

The propagation of the quantum light field through a nonlinear medium can be described by an effective one-dimensional nonlinear Schrödinger equation²⁵

$$\frac{\partial \hat{\Psi}(z, t)}{\partial t} = \left[-\frac{\partial \omega(k_0)}{\partial k} + \frac{i}{2} \frac{\partial^2 \omega(k_0)}{\partial k^2} + i\chi_e |\hat{\Psi}(z, t)|^2 \right] \hat{\Psi}(z, t), \quad (6)$$

where $\hat{\Psi}(z, t)$ is the real-space photon field operator, $\omega(k) = \frac{k}{\sqrt{\epsilon(k)\mu_0}}$ is the dispersion relation, and χ_e is the nonlinear susceptibility of the material. To solve this equation, we employ the truncated Wigner approximation (TWA), in which we construct an equivalent nonlinear stochastic equation for the \mathbf{c} -field (ψ)⁴⁹. We initialize the field with a coherent pulse containing N photons, supplemented by vacuum noise in all modes within a plane-wave basis. The observables are obtained by averaging the simulation over 10,000 stochastic trajectories on 128 spatial grid points. The photon field can be calculated as a function of propagation time t and real-space z . The one-body density matrix, $\rho(z, z') = \langle \hat{\Psi}^\dagger(z) \hat{\Psi}(z') \rangle$ ⁵⁰ is obtained from TWA simulations as

$$\rho(z, z') = \overline{\psi^*(z)\psi(z')} - \frac{1}{2}\delta(z, z') \quad (7)$$

where $\delta(z, z')$ is the delta function, subtracted due to the symmetrically ordered calculation of the correlation in Wigner function theory, and $\overline{\dots}$ denotes the stochastic average. Diagonalizing the one-body density matrix

$$\int dz' \rho(z, z') \phi_j(z') = \lambda_j \phi_j(z), \quad (8)$$

we obtain the eigenvalues (λ_j) and the corresponding eigenfunctions ($\phi_j(z)$) of the j^{th} principal mode. The multi-mode coherency matrix $(\Gamma^{(1)})_{mn} = \langle \hat{a}_m^\dagger \hat{a}_n \rangle$ in the frequency basis discussed in Eq. (1) of the main text is obtained by projecting the field operator onto the plane-wave modes $\varphi_m(z)$ as

$$\langle \hat{a}_m^\dagger \hat{a}_n \rangle = \int dz \int dz' \varphi_m^*(z) \varphi_n(z') \langle \hat{\Psi}^\dagger(z) \hat{\Psi}(z') \rangle. \quad (9)$$

Since the eigenspectrum of the coherency matrix is largely dominated by one principal mode, as shown in Fig. 5 (f), we develop an effective single-mode description. To this end, we project onto the largely occupied principal mode, $\phi(z)$, approximating the photon field as $\hat{\Psi}(z, t) \approx \phi(z) \hat{a}(t)$. Its dynamics is captured by

$$i \frac{d\hat{a}(t)}{dt} = \chi \hat{a}^\dagger(t) \hat{a}(t) \hat{a}(t). \quad (10)$$

Here, $\chi = \chi_e \int dz |\phi(z)|^4$ is the effective non-linear susceptibility for the single mode. It is directly apparent that the photon dynamics at the output only depends on $\bar{\chi} = \chi t$, the dimensionless product of nonlinearity

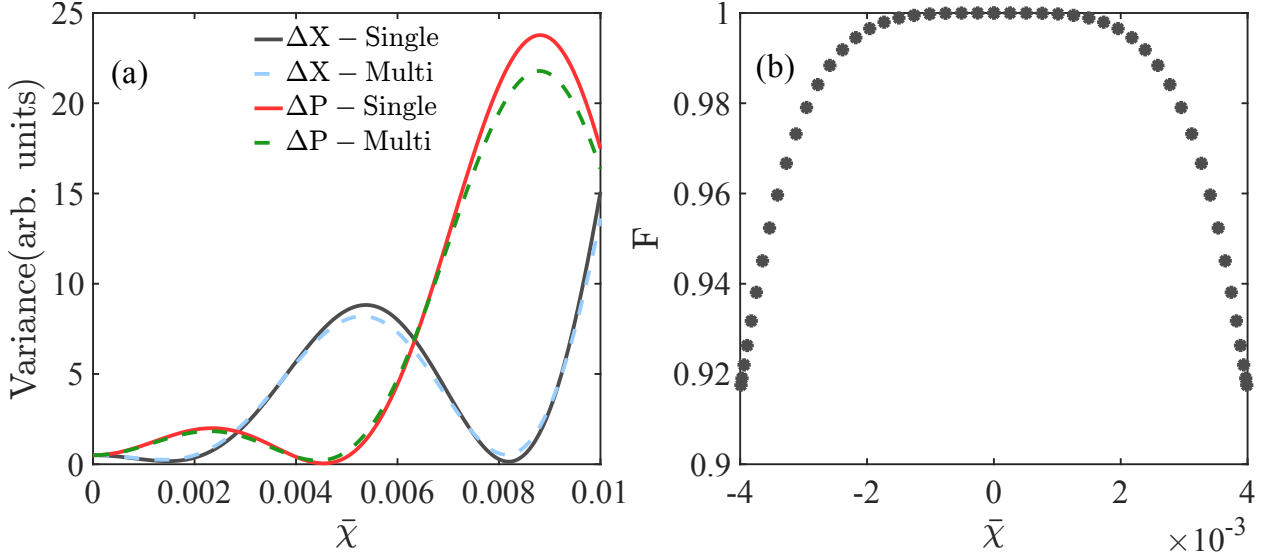


FIG. 6. Variance of the quadratures as a function of the dimensionless coupling constant $\bar{\chi}$. (a) ΔX quadrature variance obtained from the multi-mode TWA (dashed blue line) with the single-mode analytical solution (solid black line). ΔP quadrature variance from the multi-mode TWA (dashed green line) with the single-mode analytical solution (solid red line). (b) Fidelity (F) of the Gaussian approximation as a function of the dimensionless parameter $\bar{\chi}$.

and propagation time t . A comparison between the quadrature variances obtained from the full multi-mode TWA simulations and those from the analytically solved single-mode model is shown in Fig. 6 (a). In the considered limit of small $\bar{\chi}$, the single-mode model represents an excellent approximation to the full dynamics, which can be analytically solved. In the large mean-photon-number limit, the output quadrature variances emerging from a coherent input state are obtained from the single-mode model as

$$\Delta X \approx \frac{1}{2} \left[\alpha^{*2} e^{2i\bar{\chi}} e^{-2n \sin^2(2\bar{\chi})} e^{in \sin(4\bar{\chi})} + \alpha^2 e^{-2i\bar{\chi}} e^{-2n \sin^2(2\bar{\chi})} e^{-in \sin(4\bar{\chi})} + 2n + 1 \right] - 2 (\Re \langle \hat{a}(\bar{\chi}) \rangle)^2, \quad (11)$$

$$\Delta P \approx \frac{1}{2} \left[-\alpha^{*2} e^{2i\bar{\chi}} e^{-2n \sin^2(2\bar{\chi})} e^{in \sin(4\bar{\chi})} - \alpha^2 e^{-2i\bar{\chi}} e^{-2n \sin^2(2\bar{\chi})} e^{-in \sin(4\bar{\chi})} + 2n + 1 \right] - 2 (\Im \langle \hat{a}(\bar{\chi}) \rangle)^2. \quad (12)$$

Here α is the coherent-state amplitude and n is the mean photon number. Fig. 5 (e) of the main text shows these quadratures for various values of the $\bar{\chi}$. The output Wigner function for the single-mode model can also be solved exactly and analytically as⁵¹

$$W(\alpha, \bar{\chi}) = \frac{2}{\pi} e^{-2|\alpha|^2} \left[\sum_{n=0}^{\infty} (-1)^n \rho_{nn}(\bar{\chi}) L_n(4|\alpha|^2) + 2 \Re \sum_{n>m} (-1)^m \rho_{mn}(\bar{\chi}) \sqrt{\frac{m!}{n!}} (2\alpha)^{n-m} L_m^{(n-m)}(4|\alpha|^2) \right]. \quad (13)$$

Here L_m^n are the associated Laguerre polynomials and

$$\rho_{mn}(\bar{\chi}) = e^{-|\alpha|^2} \frac{\alpha^m (\alpha^*)^n}{\sqrt{m! n!}} e^{-i\bar{\chi} [m(m-1) - n(n-1)]} \quad (14)$$

are the elements of the density matrix. The Wigner function at the output exhibits negative regions characteristic of the emergence of nonclassical light (see Fig. 5). However, such nonclassical features appear only for large values of the dimensionless nonlinear parameter $\bar{\chi}$. For very small values of $\bar{\chi}$, the output state stays approximately Gaussian, and the Wigner function is well approximated by a squeezed coherent state of the form

$$W(X, P) = \frac{1}{2\pi\sqrt{\det(\Sigma)}} \exp \left[-\frac{1}{2}(\mathbf{r} - \mathbf{r}_0)^T \Sigma^{-1} (\mathbf{r} - \mathbf{r}_0) \right] \quad (15)$$

where $\mathbf{r} = (X, P)$ and $\mathbf{r}_0 = (X_{\text{mean}}, P_{\text{mean}})$. We show the fidelity (F) of the Gaussian state in Fig. 6 (b) by calculating the overlap between Eq. 13 and Eq. 15. This indicates that the state can be well approximated by a Gaussian distribution for small values of $\bar{\chi}$, where it is completely characterized by its amplitude and field quadratures.

ACKNOWLEDGEMENTS

This work was primarily supported by the U.S. Department of Energy, Office of Science, Basic Energy Sciences, under Award #DE-SC0024234. VW acknowledges support from the U.S. Department of Energy (DOE), Office of Science, Basic Energy Sciences (BES), under Award #DE-SC0026318, and by the National Science Foundation (NSF) under Award #PHYS-2409630, which supported the postdoctoral researcher SKT. C.-T.L. acknowledges support from the U.S. Air Force Office of Scientific Research (AFOSR), award no. FA9550-23-1-0234. HA acknowledges the support as part of QuPIDC, an Energy Frontier Research Center, funded by the US Department of Energy (DOE), Office of Science, Basic Energy Sciences (BES), under award number DE-SC0025620.

- ¹U. L. Andersen, T. Gehring, C. Marquardt, and G. Leuchs, “30 years of squeezed light generation,” *Physica Scripta* **91**, 053001 (2016).
- ²J. Aasi and et.al., “Enhanced sensitivity of the ligo gravitational wave detector by using squeezed states of light,” *Nature Photonics* **7**, 613–619 (2013).
- ³D. Ganapathy and et.al. (LIGO O4 Detector Collaboration), “Broadband quantum enhancement of the ligo detectors with frequency-dependent squeezing,” *Phys. Rev. X* **13**, 041021 (2023).
- ⁴E. Oelker, L. Barsotti, S. Dwyer, D. Sigg, and N. Mavalvala, “Squeezed light for advanced gravitational wave detectors and beyond,” *Opt. Express* **22**, 21106–21121 (2014).
- ⁵F. Acernese and et.al. (Virgo Collaboration), “Increasing the astrophysical reach of the advanced virgo detector via the application of squeezed vacuum states of light,” *Phys. Rev. Lett.* **123**, 231108 (2019).
- ⁶S. L. Braunstein and P. van Loock, “Quantum information with continuous variables,” *Rev. Mod. Phys.* **77**, 513–577 (2005).
- ⁷A. I. Lvovsky, “Squeezed light,” in *Photonics* (Wiley, 2015) pp. 121–163.
- ⁸P.-A. Moreau, E. Toninelli, T. Gregory, and M. J. Padgett, “Imaging with quantum states of light,” *Nature Reviews Physics* **1**, 367–380 (2019).
- ⁹C. A. Casacio, L. S. Madsen, A. Terrasson, M. Waleed, K. Barnscheidt, B. Hage, M. A. Taylor, and W. P. Bowen, “Quantum-enhanced nonlinear microscopy,” *Nature* **594**, 201–206 (2021).
- ¹⁰R. Schnabel, “Squeezed states of light and their applications in laser interferometers,” *Physics Reports* **684**, 1–51 (2017).
- ¹¹E. S. Polzik, J. Carri, and H. J. Kimble, “Spectroscopy with squeezed light,” *Physical Review Letters* **68**, 3020–3023 (1992).
- ¹²R. M. Shelby, M. D. Levenson, S. H. Perlmutter, R. G. DeVoe, and D. F. Walls, “Broad-band parametric deamplification of quantum noise in an optical fiber,” *Physical Review Letters* **57**, 691–694 (1986).
- ¹³J. W. Wu, P. K. Lam, M. B. Gray, and H.-A. Bachor, “Optical homodyne tomography of information carrying laser beams,” *Opt. Express* **3**, 154–161 (1998).
- ¹⁴M. Mehmet, S. Ast, T. Eberle, S. Steinlechner, H. Vahlbruch, and R. Schnabel, “Squeezed light at 1550 nm with a quantum noise reduction of 123 dB,” *Optics Express* **19**, 25763 (2011).
- ¹⁵W. Asavanant, K. Nakashima, Y. Shiozawa, J.-I. Yoshikawa, and A. Furusawa, “Generation of highly pure schrödinger’s cat states and real-time quadrature measurements via optical filtering,” *Optics Express* **25**, 32227 (2017).
- ¹⁶M. Lewenstein, M. F. Ciappina, E. Pisanty, J. Rivera-Dean, P. Stammer, T. Lamprou, and P. Tzallas, “Generation of optical schrödinger cat states in intense laser-matter interactions,” *Nature Physics* **17**, 1104–1108 (2021).
- ¹⁷P. Cutipa and M. V. Chekhova, “Bright squeezed vacuum for two-photon spectroscopy: simultaneously high resolution in time and frequency, space and wavevector,” *Optics Letters* **47**, 465 (2022).
- ¹⁸I. Barakat, M. Kalash, D. Scharwald, P. Sharapova, N. Lindlein, and M. Chekhova, “Simultaneous measurement of multimode squeezing through multimode phase-sensitive amplification,” *Optica Quantum* **3**, 36 (2025).
- ¹⁹A. Rasputnyi, Z. Chen, M. Birk, O. Cohen, I. Kammer, M. Krüger, D. Seletskiy, M. Chekhova, and F. Tani, “High-harmonic generation by a bright squeezed vacuum,” *Nature Physics* **20**, 1960–1965 (2024).
- ²⁰M. E. Tzur, C. Mor, N. Yaffe, M. Birk, A. Rasputnyi, O. Kneller, I. Nisim, I. Kammer, M. Krüger, N. Dudovich, and O. Cohen, “Measuring and controlling the birth of quantum attosecond pulses,” (2025).
- ²¹C. Riek, P. Sulzer, M. Seeger, A. S. Moskalenko, G. Burkard, D. V. Seletskiy, and A. Leitenstorfer, “Subcycle quantum electrodynamics,” *Nature* **541**, 376–379 (2017).
- ²²M. Sennary, J. Rivera-Dean, M. ElKabbash, V. Pervak, M. Lewenstein, and M. T. Hassan, “Attosecond quantum uncertainty dynamics and ultrafast squeezed light for quantum communication,” *Light: Science & Applications* **14** (2025), 10.1038/s41377-025-02055-x.
- ²³M. E. Tzur, C. Mor, N. Yaffe, M. Birk, A. Rasputnyi, O. Kneller, I. Nisim, I. Kammer, M. Chekhova, M. Krueger, M. Ivanov, N. Dudovich, and O. Cohen, “Attosecond-resolved quantum fluctuations of light and matter,” (2025).

²⁴H. Bachor and T. C. Ralph, *A Guide to Experiments in Quantum Optics* (Wiley, 2019).

²⁵P. D. Drummond and M. Hillery, *The Quantum Theory of Nonlinear Optics* (Cambridge University Press, 2014).

²⁶P. G. Kwiat, K. Mattle, H. Weinfurter, A. Zeilinger, A. V. Sergienko, and Y. Shih, “New high-intensity source of polarization-entangled photon pairs,” *Phys. Rev. Lett.* **75**, 4337–4341 (1995).

²⁷P. Kumar and J. H. Shapiro, “Squeezed-state generation via forward degenerate four-wave mixing,” *Phys. Rev. A* **30**, 1568–1571 (1984).

²⁸R. S. Bondurant, P. Kumar, J. H. Shapiro, and M. Maeda, “Degenerate four-wave mixing as a possible source of squeezed-state light,” *Physical Review A* **30**, 343–353 (1984).

²⁹B. L. Schmittberger Marlow, “Degenerate four-wave-mixing as a low-power source of squeezed light,” *Optics Express* **28**, 38169 (2020).

³⁰M. E. Marhic and C.-H. Hsia, “Optical amplification and squeezed-light generation in fibre interferometers performing degenerate four-wave mixing,” *Quantum Optics: Journal of the European Optical Society Part B* **3**, 341–358 (1991).

³¹H. Vahlbruch, M. Mehmet, K. Danzmann, and R. Schnabel, “Detection of 15 db squeezed states of light and their application for the absolute calibration of photoelectric quantum efficiency,” *Physical Review Letters* **117** (2016), 10.1103/physrevlett.117.110801.

³²F. Walz, S. Kumar, A. S. Olounabadi, Y. Zhong, R. Zimmerman, S. Pandey, E. Liu, L. Z. Tan, and N. Shivaram, “Strong-field driven sub-cycle band structure modulation measured with ultrafast electric field observables,” (2025).

³³C. Fabre and N. Treps, “Modes and states in quantum optics,” *Reviews of Modern Physics* **92** (2020), 10.1103/revmodphys.92.035005.

³⁴J. Roslund, R. M. de Araújo, S. Jiang, C. Fabre, and N. Treps, “Wavelength-multiplexed quantum networks with ultrafast frequency combs,” *Nature Photonics* **8**, 109–112 (2013).

³⁵S. Ghimire, A. D. DiChiara, E. Sistrunk, P. Agostini, L. F. DiMauro, and D. A. Reis, “Observation of high-order harmonic generation in a bulk crystal,” *Nature Physics* **7**, 138–141 (2011).

³⁶M. Orszag, *Quantum Optics* (Springer International Publishing, 2016).

³⁷G. S. Agarwal, *Quantum Optics* (Cambridge University Press, 2012).

³⁸H. H. Adamyan, J. A. Bergou, N. T. Gevorgyan, and G. Y. Kryuchkyan, “Strong squeezing in periodically modulated optical parametric oscillators,” *Phys. Rev. A* **92**, 053818 (2015).

³⁹J. R. Álvarez, A. Martínez, and A. Valencia, “Measuring wigner functions of quantum states of light in the undergraduate lab,” in *Seventeenth Conference on Education and Training in Optics and Photonics: ETOP 2023*, edited by D. J. Hagan and M. McKee (SPIE, 2023) p. 27.

⁴⁰A. Kenfack and K. yczkowski, “Negativity of the wigner function as an indicator of non-classicality,” *Journal of Optics B: Quantum and Semiclassical Optics* **6**, 396–404 (2004).

⁴¹R. Dahan, A. Gorlach, U. Haeusler, A. Karnieli, O. Eyal, P. Yousefi, M. Segev, A. Arie, G. Eisenstein, P. Hommelhoff, and I. Kaminer, “Imprinting the quantum statistics of photons on free electrons,” *Science* **373** (2021), 10.1126/science.abj7128.

⁴²V. Gruzdev and O. Sergaeva, “Ultrafast modification of band structure of wide-band-gap solids by ultrashort pulses of laser-driven electron oscillations,” *Phys. Rev. B* **98**, 115202 (2018).

⁴³A. J. Uzan-Narovlansky, Á. Jiménez-Galán, G. Orenstein, R. E. Silva, T. Arusi-Parpar, S. Shames, B. D. Bruner, B. Yan, O. Smirnova, M. Ivanov, *et al.*, “Observation of light-driven band structure via multiband high-harmonic spectroscopy,” *Nature photonics* **16**, 428–432 (2022).

⁴⁴M. Lucchini, S. A. Sato, A. Ludwig, J. Herrmann, M. Volkov, L. Kasmi, Y. Shinohara, K. Yabana, L. Gallmann, and U. Keller, “Attosecond dynamical fritz-keldysh effect in polycrystalline diamond,” *Science* **353**, 916–919 (2016), <https://www.science.org/doi/pdf/10.1126/science.aag1268>.

⁴⁵M. Even Tzur, M. Birk, A. Gorlach, M. Krüger, I. Kaminer, and O. Cohen, “Photon-statistics force in ultrafast electron dynamics,” *Nature Photonics* **17**, 501–509 (2023).

⁴⁶X. Long, P. Li, and Y. Liu, “Hydrogen molecular dissociation driven by quantum light,” *Phys. Rev. Lett.* **135**, 153201 (2025).

⁴⁷J. A. Shirley, R. J. Hall, and A. C. Eckbreth, “Folded boxcars for rotational raman studies,” *Opt. Lett.* **5**, 380–382 (1980).

⁴⁸C. Navarrete-Benlloch, “Introduction to quantum optics,” (2022).

⁴⁹P. Blakie, A. Bradley, M. Davis, R. Ballagh, and C. Gardiner, “Dynamics and statistical mechanics of ultra-cold bose gases using c-field techniques,” *Advances in Physics* **57**, 363–455 (2008).

⁵⁰C. J. Pethik and H. Smith, *Bose-Einstein condensation in dilute gases* (Cambridge University Press, 2002).

⁵¹J. C. L. Carreño, “Wigner function of observed quantum systems,” *New Journal of Physics* **27**, 043009 (2025).

SUPPLEMENTARY INFORMATION

Nonlinear response filtering

Here, we present detailed plots of the homodyne signal, fully characterized as a function of the local oscillator phase ϕ_{LO} for various time delays. The raw data (unfiltered) are shown in Fig. 7 (a). Figure 7 (c) displays the signal for a specific value of ϕ_{LO} . A Fourier transform is performed along the time-delay axis, followed by the application of a low-pass filter to retain frequency components corresponding to $\omega \leq 1\omega_0$, as illustrated in Fig. 7 (d). The higher-order components are treated as noise. Repeating this procedure for all values of ϕ_{LO} yields a denoised, fully characterized homodyne signal, shown in Fig. 7 (b).

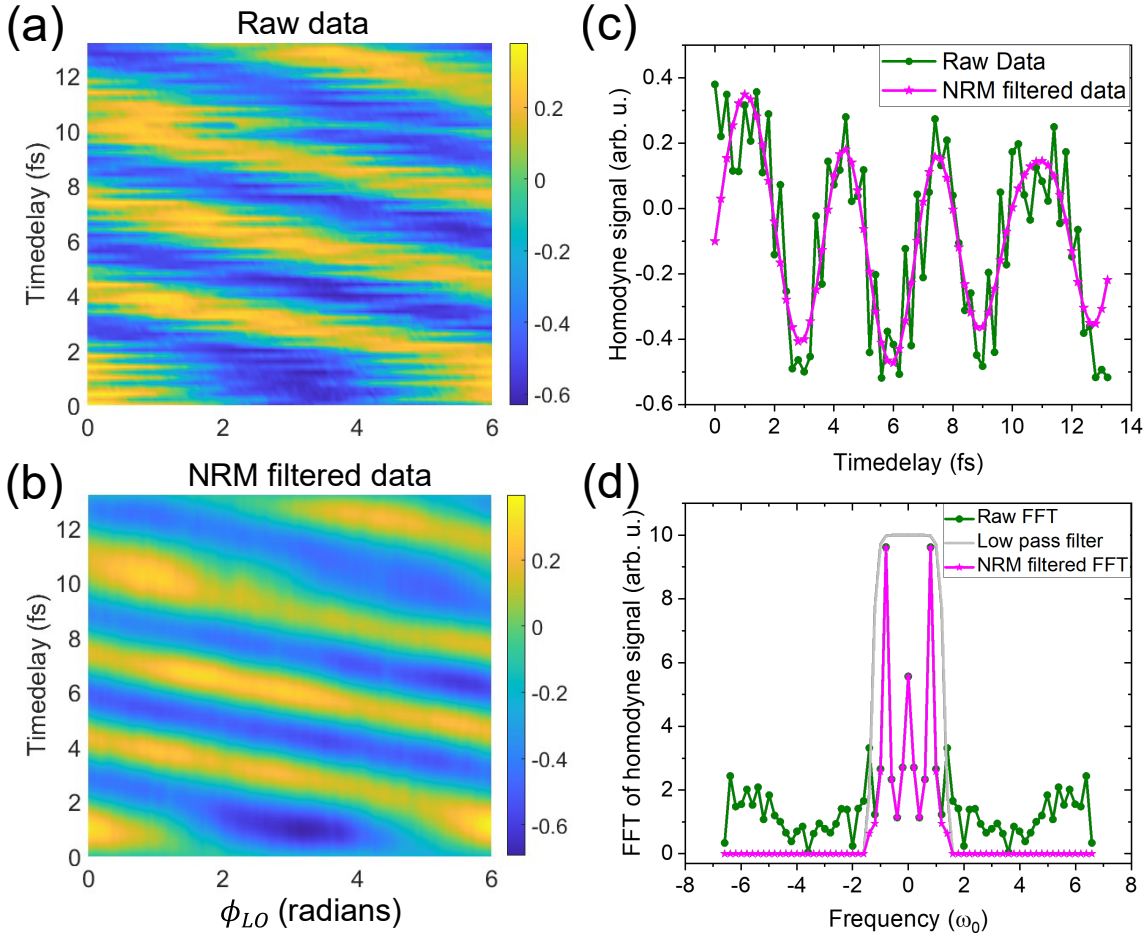


FIG. 7. The averaged homodyne signal (a) raw and (b) NRM filtered data as a function of the phase of the local oscillator (ϕ_{LO}) and time delay between gate and the probe. (c) shows the raw (green) and filtered (magenta) data as a function of time delay for $\phi_{LO} = 0$ and (d) is its Fourier transformation showing $1\omega_0$ oscillation in time delay where ω_0 is the laser central frequency. We filter the raw data (green) by applying a low-pass filter (grey), which excludes all higher-order oscillation noises in the filtered signal (magenta).

Quadrature and Noise correlations

As discussed in the main text, because we have the ability to measure the frequency resolved homodyne detection, it is possible to measure the quadrature correlation of the DFWM signal. The various quadrature

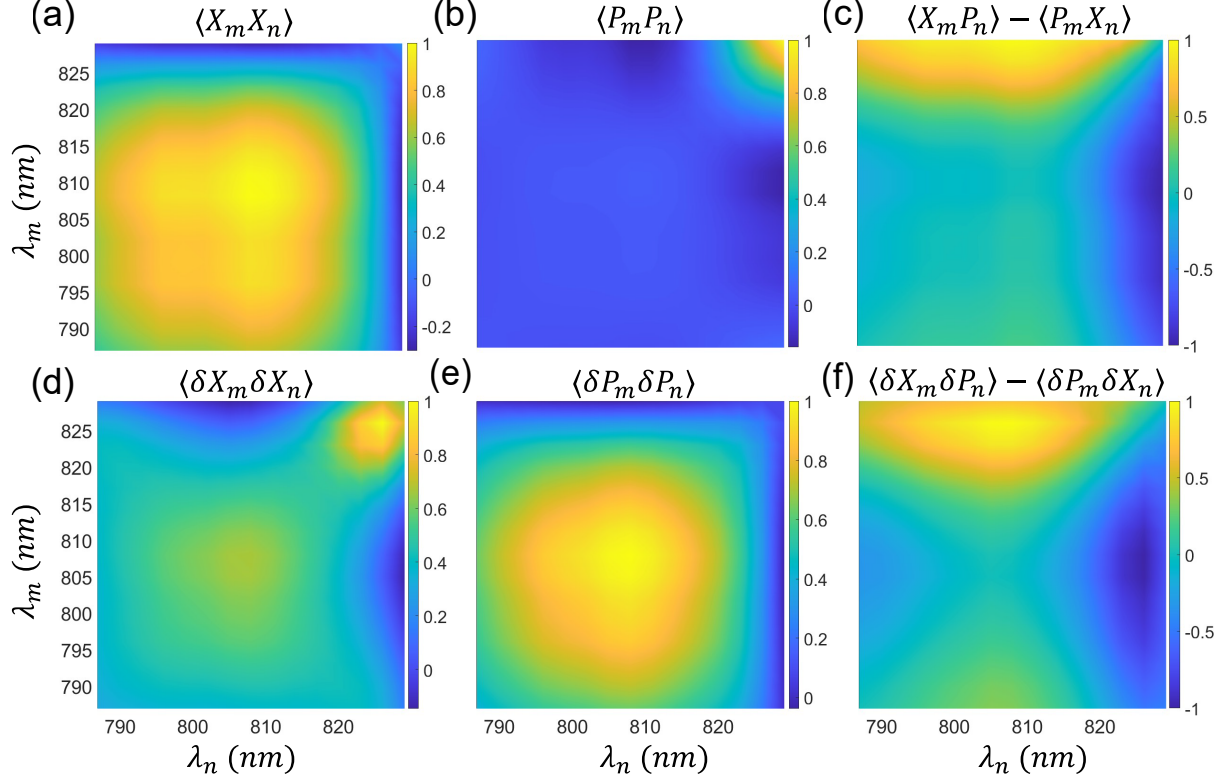


FIG. 8. The elements of the covariance matrix are shown here for the amplitude squeezed state at $\tau = 10.2$ fs. The diagonal terms (a) $\langle X_m X_n \rangle$ and (b) $\langle P_m P_n \rangle$ and the difference in off diagonal terms (c) $\langle X_m P_n \rangle - \langle P_m X_n \rangle$. Similarly, correlation functions of quadrature noise are shown here (d) $\langle \delta X_m \delta X_n \rangle$ (e) $\langle \delta P_m \delta P_n \rangle$, and (f) $\langle \delta X_m \delta P_n \rangle - \langle \delta P_m \delta X_n \rangle$.

correlations, in addition to those shown in figure 4 in the main text, are shown here in Fig. 8 (a) - (c). We can also extract the quantum noise correlations between different quadratures defined by $\langle \delta X_m \delta X_n \rangle$, $\langle \delta P_m \delta P_n \rangle$, $\langle \delta X_m \delta P_n \rangle$, and $\langle \delta P_m \delta X_n \rangle$. The corresponding noise correlations are plotted in Fig. 8 (d) - (f).

2D Gaussian fitting of Wigner function

To quantify the quadrature squeezing, we fit a generalized two-dimensional gaussian function to the measured Wigner function (see the main text for details). The measured Wigner function for $\tau = 1.2, 4.8, 7.6, 8.2$ fs is shown in Fig. 9 (a) - (d), respectively. Their corresponding fitted functions are shown in Fig. 9 (e) - (h), respectively.

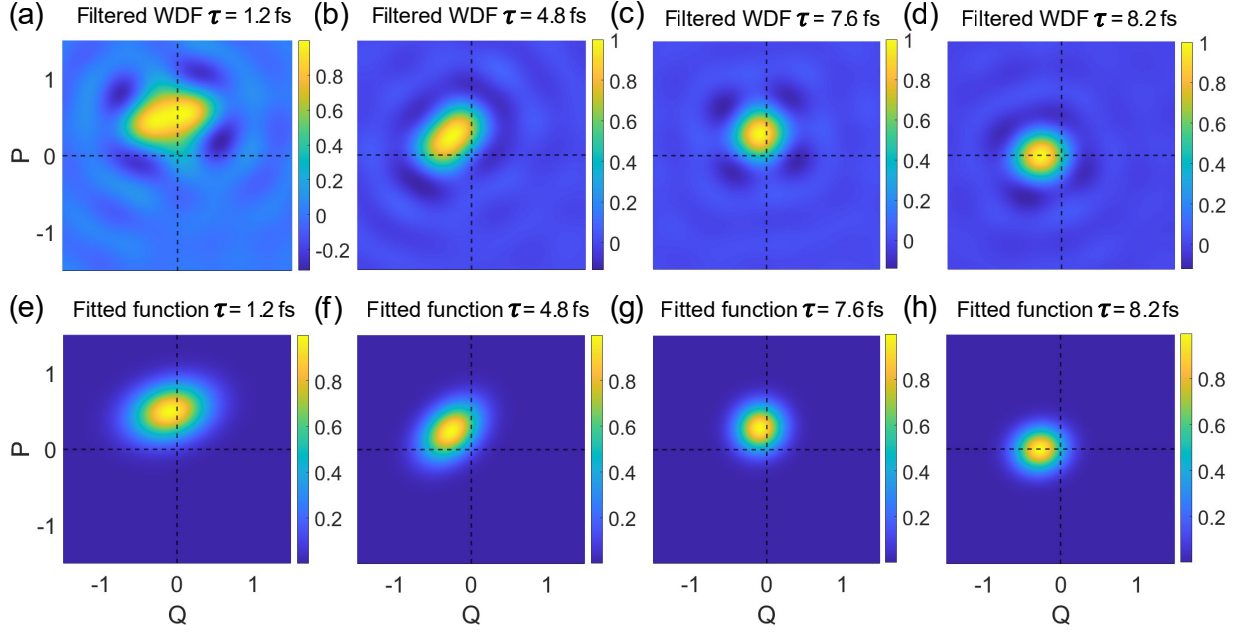


FIG. 9. The experimental NRM filtered Wigner distribution function (WDF) for time delay τ = (a) 1.2 fs (b) 4.8 fs (c) 7.6 fs and (d) 8.2 fs. The corresponding Wigner functions are fitted to a generalized 2D gaussian function shown in (e) - (h), respectively. The centroid of the Wigner distribution moves for different time delays due to a global phase of the signal with respect to the local oscillator.